buildings

MDPI

Article

Computationally Efficient Method for Steel Column Buckling in Fire

Andrei Kervalishvili and Ivar Talvik *

Department of Civil Engineering and Architecture, Tallinn University of Technology, Ehitajate tee 5, 19086 Tallinn, Estonia
* Correspondence: ivar.talvik@taltech.ee

Abstract: The stability of axially loaded steel columns with compact rectangular hollow sections at elevated temperatures is studied in this paper. The current Eurocode model for checking the buckling resistance of columns in fire was developed on a similar basis to that for ambient conditions. Due to the effect of the complex non-linear behaviour of steel in fire, the standard design model is not always fully appropriate, and certain parameter ranges may give unsafe results. In this work, an analytical method to determine the buckling resistance of steel columns at elevated temperatures is proposed, accounting for variable non-linear stiffness properties which have significant effects on the flexural buckling resistance of steel columns in fire. A finite element model was developed, and an extensive numerical study was performed to explore the effects of different parameters on the behaviours of steel columns at elevated temperatures. The proposed method is validated by comparing the performance with the results of the numerical model. Its improved accuracy with respect to the current Eurocode method is verified. The advantage of the new technique is its computational efficiency, which is valuable in reliability evaluations or data-based design procedures demanding numerous calculation cycles. The potential of the method for probability-based analysis is supported by the format, which enables us to explicitly handle the uncertainties of essential parameters. The proposed framework is suitable for extension to incorporate different material models and section types.

Keywords: column; buckling; fire; Eurocode 3; analytical model; numerical analysis

Citation: Kervalishvili, A.; Talvik, I. Computationally Efficient Method for Steel Column Buckling in Fire. *Buildings* **2023**, *13*, 407. https://doi.org/10.3390/buildings13020407

Academic Editor: Gang Zhang

Received: 14 December 2022
Revised: 22 January 2023
Accepted: 25 January 2023
Published: 2 February 2023

1. Introduction

Columns should be treated with special care in building design, as their capacity is vital when considering potential progressive collapse of the structural frame. Column resistance is most likely to be affected by instability phenomena. The buckling of axially loaded columns is a substantial subtask within the overall set of column stability issues. Studies of steel column stability at ambient temperatures have been thoroughly reported. In recent years, considerable efforts in structural engineering research have been made to address fire conditions. Compared to ambient conditions, the structural behaviour of steel columns at elevated temperatures becomes more complex due to the temperature-dependent stress–strain relationship of the material. Numerical methods have been proven to produce reliable results in various tasks for structural behaviour in fire. For practical design purposes, a relevant Eurocode [1] procedure is available, initially proposed by Franssen [2]. The current Eurocode method related to the buckling capacity of columns in fire is based on extensive experimental [2] and numerical investigations [3]. Certain discrepancies between the Eurocode EN 1993-1-2 [1] method and the results of experimental work, as well as numerical modelling, have been reported by different authors. Knobloch et al. [4] and Somaini et al. [5] point out that the simplified design approach, although convenient for use, does not properly account for material nonlinearity at elevated temperatures. Reduced accuracy may also be caused by the extrapolation of the hot-rolled H-section data to other

various profiles, such as hollow sections, as concluded by Vila Real et al. [6]. Several authors, such as Somaini et al. [5], Toh et al. [7] and Kervalishvili and Talvik [8], have pointed out that, in certain parameter ranges, the Eurocode design results may appear nonconservative.

In recent years, along with the development of computational capacity and relevant methods, the probabilistic design approach has been introduced as an alternative procedure to address the safety level and reliability of structures, especially in performance-based design methodology [9]. Relevant research reports deal with different structural elements, and the reliability of compression elements has been studied at normal temperatures and in fire conditions [10–13]. A reliability-based approach has been used to account for uncertainties in order to achieve the optimised solution of structures of inherently nonlinear character [14]. Evaluating the safety of structures with probabilistic methods in various limit states requires the intensive analysis of structural models. A high number of repeated samples of the model with random input values accounting for uncertainties is necessary for the commonly used Monte Carlo simulation method. There is a similar need for a high number of repeated calculations applied to emerging data-based techniques of structural assessment [15]. Although the finite element method (FEM) has been widely used and approved as a sufficiently accurate method to reproduce the behaviour of structures under extreme damage effects, such as fire, its use for the adequate number of iterations in probabilistic methods appears to be costly in terms of time and may be impractical to apply [9,16]. Various simplifying methods are not always sufficiently accurate or convenient to use [12,16]. Consequently, there is a growing need for methods that provide both adequate accuracy and computational efficiency for structural analysis in fire.

In the present work, a computationally efficient capacity verification method for axially loaded steel columns with rectangular hollow section (RHS) and square hollow section (SHS) with section classes 1 and 2 (as defined in [1]) in fire conditions is proposed. Numerical modelling is conducted to verify the accuracy of the method compared to EN 1993-1-2 based results. Computational efficiency of the method is assessed by comparison with the finite element model. The reported analytical procedure is derived on the basis of nonlinear material model. In this way, the stiffness properties can be regarded in detail and it is possible to incorporate different materials in the same framework. The format of the proposed technique is specifically suitable for reliability analysis as the relevant parameters with uncertainties can be explicitly handled in the procedure.

2. Alternative Methods for Column Buckling in Fire

The EN 1993-1-2 [1] design method for axially loaded columns in fire conditions is, in principle, a modified version of the method for similar problems in ambient temperature conditions, which is based on first-yield criterion [17]. The criterion was introduced by Ayrton and Perry [18] as follows: an initially curved column loses stability when maximum compression stresses on the concave side in the mid-height section of the column approach the yield limit value. EN 1993-1-2 uses the Ayrton–Perry framework for buckling capacity estimation of axially loaded elements, which is modified to fit the model to the experimental results [2], and extensive numerical investigation by Talamona et al. [3], as presented by Schleich et al. [19].

An alternative approach based on a Rankine-type solution was proposed by Toh et al. [7] and Maślak [20]. The solution is presented in compact analytical form and the predicted buckling capacity is close to the result predicted by the EN 1993-1-2 method. Capacity estimation of a restrained steel column in fire conditions was proposed by Neves et al. [21] and Wang et al. [22]. Von Karman type method for steel column buckling in fire was presented by Somaini [5]. The method proposed in this work is also based on the Von Karman solution.

The Von Karman method focuses on the equilibrium between the external bending moment and the internal bending moment in the critical section [23]. The initial imperfect shape of a column is approximated by a sinusoidal curve (Figure 1, Equation (1)); the

amplitude is denoted as $y_{0.mid}$. Lateral displacement (Equation (2)) develops with the increasing axial load N_e, and the eccentricity of the axial load increases from $y_{0.mid}$ to $y_{tot.mid}$ = $y_{0.mid}$ + $y_{1.mid}$, where $y_{0.mid}$ and $y_{1.mid}$ are shown in Figure 1. This process obviously leads to an increase in the bending moment, as shown in Equation (3). The column remains stable until the increase in the external bending moment M_e is fully compensated by the increase in the internal bending moment M_i and the load N_e is equal to the internal force N_i. Stability criteria can be formulated as Equation (4). Generally, the internal bending moment M_i and the internal axial force N_i are interconnected. Section curvature χ links M_i and $y_{tot.mid}$. For a column with pinned ends, the mid-height section curvature and the maximum lateral deflection are linked with Equations (5) and (6), where ε_1 and ε_2 are the strains at the section extreme points and h is the section height. If the strains are available, the internal forces of the section can be calculated for elastic state, but it is not the case for steel in fire conditions. Using Equations (4)–(6), and using the dependences of M_i and N_i on the strains ε_1 and ε_2, it is possible to define the buckling load limit of a column. Due to the complicated nature of the steel material law in fire conditions, the analytical model for Equation (4) is not so easy to establish. The Von Karman method can be effectively used in the numerical procedure with section discretisation, but computational efficiency of the method does not outperform finite element formulation.

$$y_0 = y_{0.mid} \sin\left(\frac{\pi x}{L}\right) \tag{1}$$

$$y_1 = y_{1.mid} \sin\left(\frac{\pi x}{L}\right) \tag{2}$$

$$M_e = N_e y_{tot.mid} \tag{3}$$

$$\frac{dM_e}{dy_{tot.mid}} \leq \frac{dM_i}{dy_{tot.mid}} \tag{4}$$

$$\chi = y_1 \left(\frac{\pi}{L}\right)^2 \tag{5}$$

$$\chi = \frac{\varepsilon_2 - \varepsilon_1}{h} \tag{6}$$

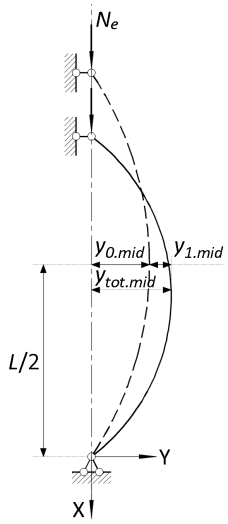

Figure 1. Column with initial imperfection.

3. Numerical Modelling

The finite element method (FEM) is widely used for analysing the buckling phenomenon of steel structures in fire conditions. The design method proposed in this work also utilises the simulation results of a nonlinear FEM model. Aspects of numerical modelling of the problem under consideration are well known. Therefore, only a short summary

of the modelling is presented herein and more details can be found in [8]. The model consisted of 20 non-linear beam elements along the column axis. Section meshing was used to calculate the section stiffness and internal forces. Temperature-dependent material models (thermal elongation and stress–strain relationships) from EN 1993-1-2 [1] were implemented. Initial curvature was taken as a half sinusoidal wave in accordance with [24]. The influence of residual stresses was considered in accordance with [24].

$$\lambda_{20°C} = \frac{L}{i\,\pi}\sqrt{\frac{f_{y.20°C}}{E_{20°C}}} \tag{7}$$

The program of numerical studies consisted of six sections (Table 1). Fifteen slenderness (see Equation (7)) values were selected to model the columns in eight temperature ranges. Steel grades S235, S355 and S460 were used for all specimens. The total number of analysed FEM models was 2160.

Table 1. Sections used for numerical modelling.

Section Type	Profile	Axis
RHS	SHS50 × 3	-
	SHS160 × 6	-
	SHS300 × 12	-
	RHS80 × 60 × 4	Strong
	RHS150 × 100 × 6	Strong
	RHS300 × 150 × 10	Strong

The results of the numerical simulations are reported here in brief. Firstly, the difference between the buckling factors of different section profiles is addressed. Table 2 presents the results of statistical analysis comparing the buckling factors for individual sections χ_i with the mean for the whole set of sections $\chi_{gr.mean}$ (factor $\chi_i/\chi_{gr.mean}$). It is obvious that the responses of columns with different section profiles are rather similar. Buckling factors obtained by the FEM (χ_{FEM}) and the EN 1993-1-2 methods (χ_{EC}) are compared in Figure 2. Deviations between the non-linear FEM and EN 1993-1-2 results can be observed and are in line with similar results reported earlier in [4,6,8].

Table 2. Descriptive statistics for individual buckling factor vs. average buckling factor for the whole set.

Steel Grade	S235	S355	S460
Mean	1.00008	1.00008	1.00005
Standard Error	0.00010	0.00009	0.00010
Standard Deviation	0.00057	0.00064	0.00066
Minimum	0.99013	0.99203	0.99119
Maximum	1.00986	1.00912	1.00949

Stresses at the limit load at the characteristic section points along the column axis are presented in Figure 3. Point 1 is located at the outer edge of the section on the side of the column, where lateral deflection causes tension; Point 2 is located at the outer edge of the section on the side of the column, where lateral deflection causes compression; and Point C is located at the centre of gravity of the section. The stresses are presented in relation to the proportionality limit for the respective temperature. Three slenderness values and three temperatures were addressed. It is evident that the stress state at failure varies with both temperature and slenderness: for a low slenderness value ($\lambda_{20°C}$ = 0.1) and for all temperatures, the stresses in the column at failure are above the proportionality limit; for a high slenderness value ($\lambda_{20°C}$ = 2.0) and for temperatures θ = 200 °C and θ = 500 °C, buckling took place when the maximum stresses approached the proportionality limit

(first-yield criterion); while for θ = 900 °C, buckling takes place elastically; with a moderate slenderness value ($\lambda_{20°C}$ = 1.0), buckling took place when the section was partially in a plastic state, and the extent of plastification varied with temperature.

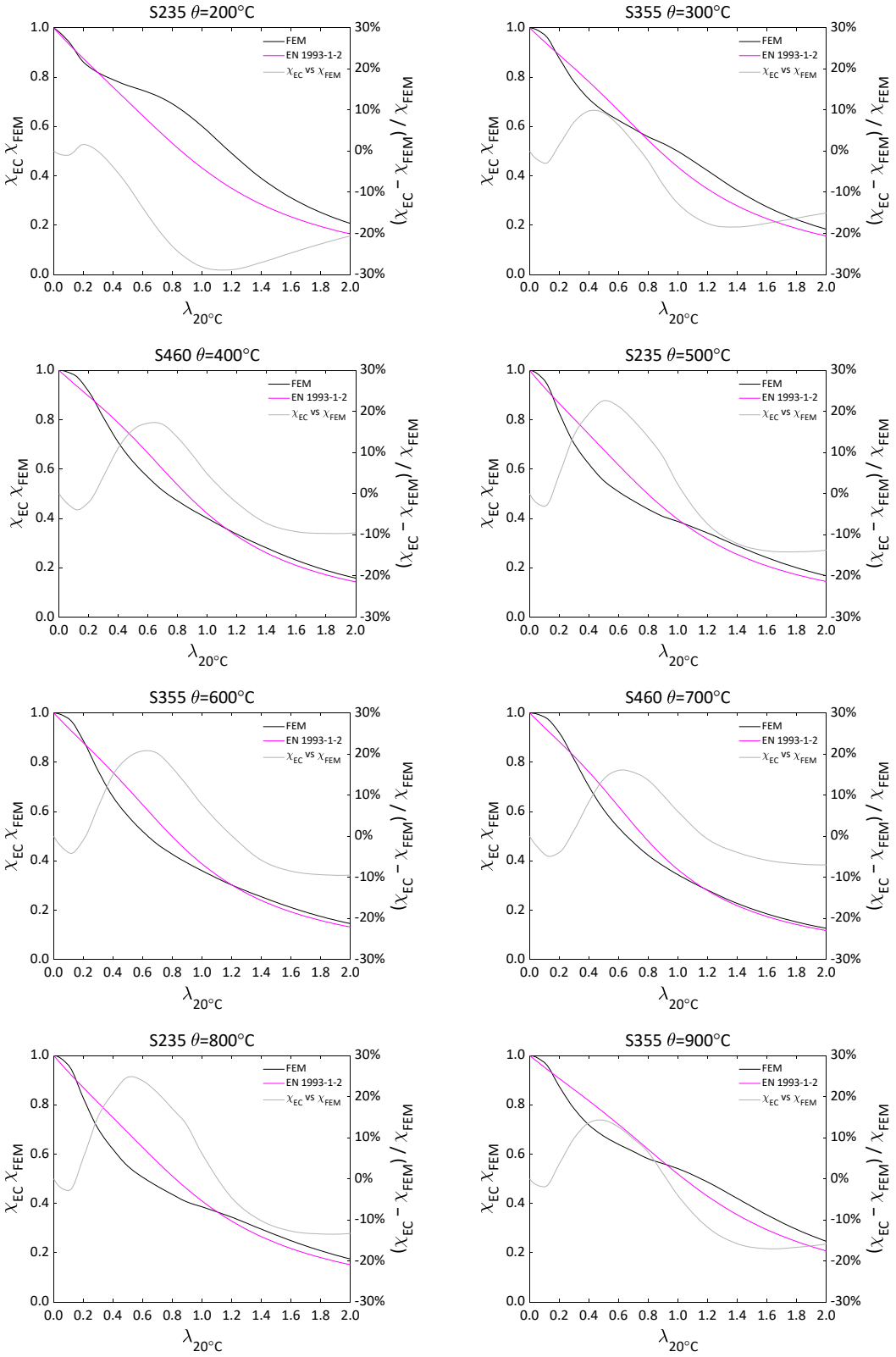

Figure 2. Buckling factors obtained by FEM vs. EN 1993-1-2 for different steel grades and heating temperatures.

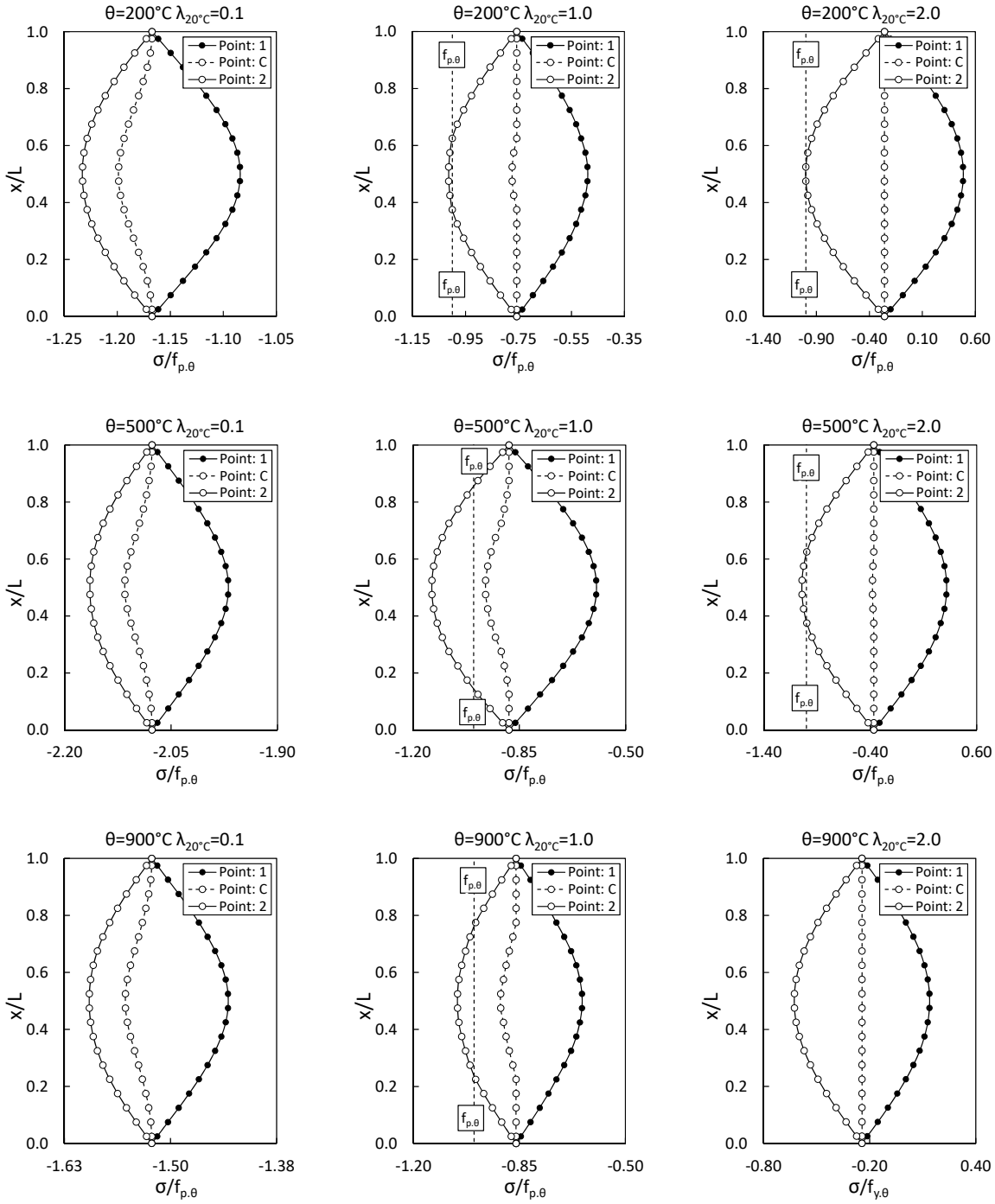

Figure 3. Stress distributions at buckling of SHS160x6 S355 for different slenderness ratios and heating temperatures.

The path of strains at Points 1, 2 and C of the mid-height section is presented in Figure 4. With increasing the axial load, the strains start to diverge intensively when approaching the buckling load. It is worth noting that, at Point 1 of the section, the unloading only took place in the very vicinity of the buckling occurrence.

The method proposed in this work was based on and validated by the results obtained by FEM. Results obtained by FEM were validated by the test results of ETHZ [25].

Tests in ETHZ [25] were performed in 2012 on a limited number of columns, including I-sections with buckling about the weak and strong axes and RHS sections. Tests were organised in the load domain, i.e., columns were heated uniformly up to a given tem-

perature and then loaded until collapse. The tests were accompanied by material tests and accurate data regarding stress–strain relationships, which are very important for the validation of the numerical model. The validation results are presented in Figure 5 and Table 3. In Table 3, the following notation is used: ID is the test identifier in the ETHZ [25] test report; f_y is the actual yield limit stress in ambient conditions; F_{ult} is the ultimate load; σ_c is the stress from the axial load; $f_{y.fi}$ is the yield limit stress corresponding to the temperature at failure calculated in accordance with EN 1993-1-2 [1]; χ_{test} is the buckling factor according to the test result; χ_{FEM} is the buckling factor calculated by FEM; and θ_{test} is the average temperature at failure according to the test results. By analysing the results of the validation, it can be concluded that good correlations with the ETHZ [25] test were achieved.

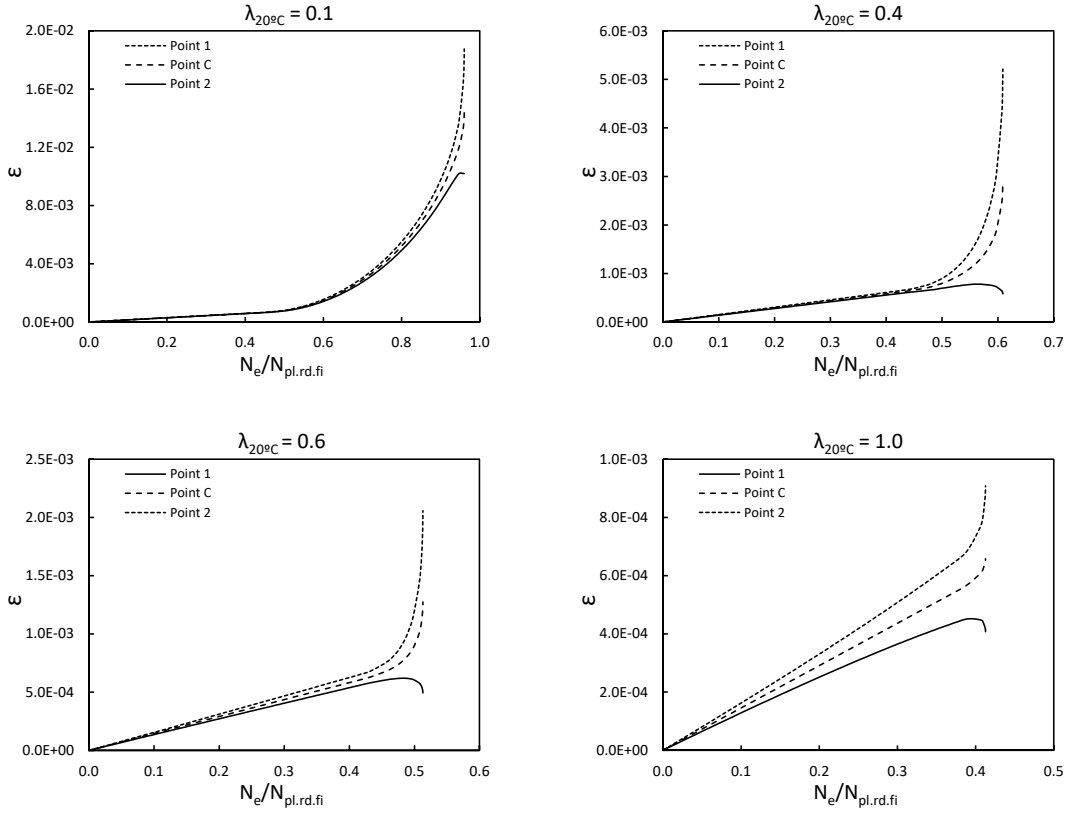

Figure 4. Mid-height section strain paths for RHS160x6 S355 with different slenderness ratios at θ = 500 °C.

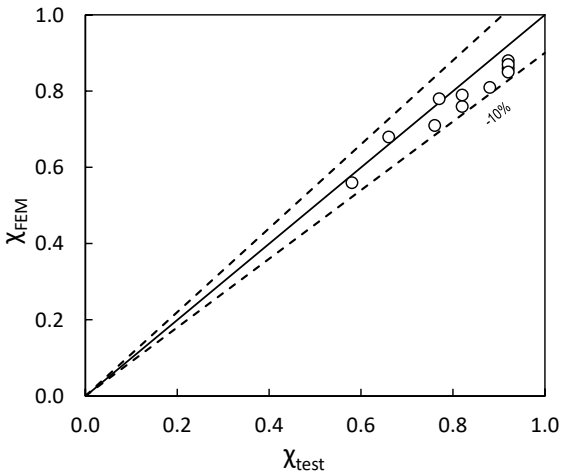

Figure 5. Validation of the numerical results against the test results.

Table 3. Validation of the numerical results against the test series from ETHZ [25].

ID	Profile	Axis	L_{eff}, mm	$f_{y.fi}$, MPa	θ_{test}, °C	F_{ult}, kN	χ_{test}	χ_{FEM}	χ_{FEM}/χ_{Test}
L2	SHS 160 × 5.0	strong	1 981	284	400	760	0.82	0.76	0.93
L5	SHS 160 × 5.0	strong	1 983	155	550	467	0.92	0.86	0.93
L6	SHS 160 × 5.0	strong	1 983	43	700	130	0.92	0.88	0.96
L08	HEA 100	strong	1 921	356	400	608	0.76	0.71	0.94
L07	HEA 100	strong	1 920	198	550	395	0.88	0.81	0.92
L01	HEA 100	strong	1 921	73	700	152	0.92	0.87	0.94

4. Proposed Design Method

The proposed method is based on the Von Karman solution described in Section 2.

In the case of an axially loaded column with pinned supports and sinusoidal initial shape, it is sufficient if the condition described by Equation (4) is checked only in the mid-section of the column, where the maximum lateral displacement occurs. The relationship between the lateral displacement and the mid-section curvature is established by Equation (5). In fire conditions, the stress distribution across the section is not linear and the calculation of the internal forces is a complex task. Destabilising forces can be expressed as Equation (3).

The mid-section of the column under consideration is presented in Figure 6. The following initial assumptions are made:

- the Navier–Bernoulli (plane sections) hypothesis is valid;
- the Eurocode [1] material model is valid;
- Point 1 is subjected to additional compression as a result of the lateral displacement, and, in contrast, Point 2 is subjected to unloading as a result of the lateral displacement.

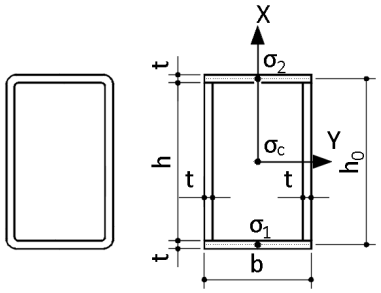

Figure 6. Column section scheme.

The following description of the formulation is rather simple in essence, but is relatively lengthy and may seem burdensome. The authors are aware of such a risk, but it is provided for the sake of completeness of the method presentation.

The internal forces of the section are defined as follows. An assumption is made as indicated in Equation (8): linear stress variation across the section is assumed, which automatically means that the stress σ_c at the centroid is equal to the mean value of stresses at Points 1 and 2 presented in (8). The internal axial force N_i is split into components as shown in Equation (9): force in the flanges, according to Equations (10) and (11), and force in the wall according to Equation (12).

$$\sigma_c = \frac{\sigma_1 + \sigma_2}{2} \tag{8}$$

$$N_i = N_{i.1} + N_{i.2} + N_{i.3} \tag{9}$$

$$N_{i.1} = \sigma_1 bt \tag{10}$$

$$N_{i.2} = \sigma_2 bt \tag{11}$$

$$N_{i.3} = \frac{ht}{6}(\sigma_1 + 4\sigma_c + \sigma_2) = \sigma_1\frac{ht}{2} + \sigma_1\frac{ht}{2} \tag{12}$$

The Simpson integration scheme was used for the section wall. Total internal axial force is given in Equation (13):

$$N_i = \sigma_1\left(bt_1 + \frac{ht}{2}\right) + \sigma_2\left(bt_1 + \frac{ht}{2}\right) = \sigma_1\alpha_1 + \sigma_2\alpha_2 \tag{13}$$

Factors α_1 and α_2 are introduced as Equations (14) and (15).

$$\alpha_1 = bt + \frac{ht}{2} \tag{14}$$

$$\alpha_2 = bt + \frac{ht}{2} \tag{15}$$

The internal bending moment is formulated in Equations (16)–(19).

$$M_i = M_{i.1} + M_{i.2} + M_{i.3} \tag{16}$$

$$M_{i.1} = -\sigma_1 bt\frac{h_0}{2} \tag{17}$$

$$M_{i.2} = -\sigma_2 bt\frac{h_0}{2} \tag{18}$$

$$M_{i.3} = \frac{ht}{6}\left(-\sigma_1\frac{h}{2} + \sigma_2\frac{h}{2}\right) = \sigma_2\frac{h^2t}{12} - \sigma_1\frac{h^2t}{12} \tag{19}$$

Factor β is introduced as Equation (20):

$$\beta = bt\frac{h_0}{2} + \frac{h^2t}{12} \tag{20}$$

The internal bending moment can then be rewritten as Equation (21):

$$M_i = \sigma_2\left(\frac{h^2t}{12} + bt_1\frac{h_0}{2}\right) - \sigma_1\left(\frac{h^2t}{12} + bt_1\frac{h_0}{2}\right) = \sigma_2\beta - \sigma_1\beta \tag{21}$$

The stress at Point 1 is expressed through the stress at Point 2, assuming the internal force (N_i) and the external axial forces (N_e) are in equilibrium (Equation (22)). It is assumed that stresses at Point 1 follow the Eurocode [1] material model. Then, Equation (22) can be rewritten as Equation (23):

$$-N_e = N_i = \sigma_1\alpha_1 + \sigma_2\alpha_2 \rightarrow \sigma_1 = -\frac{N_e}{\alpha_1} - \frac{\alpha_2}{\alpha_1}\sigma_2 \tag{22}$$

$$-f_{p.\theta} + c_{EC} - \frac{b_{EC}}{a_{EC}}\sqrt{a_{EC}^2 - \left(\varepsilon_{y.\theta} + \varepsilon_1\right)^2} = -\frac{N_e}{\alpha_1} - \frac{\alpha_2}{\alpha_1}\sigma_2 \tag{23}$$

In Equation (23), and further following the EN 1993-1-2 [1] material model, the following notations are used: $f_{p.\theta}$—proportionality limit stress at temperature θ; $\varepsilon_{y\cdot\theta}$—yield strain; a_{EC}, b_{EC} and c_{EC}—identical to the parameters a, b and c of the EN 1993-1-2 [1] material model. For a pin-ended column with sinusoidal initial curvature, the total lateral displacement at the mid-height can be expressed as a function of the section curvature—Equation (24):

$$y_{tot} = y_0 + \frac{\varepsilon_2 - \varepsilon_1}{h_0}\left(\frac{L}{\pi}\right)^2 = y_0 + (\varepsilon_2 - \varepsilon_1)\chi_0 \tag{24}$$

Parameter χ_0 is introduced as Equation (25) for convenience.

$$\chi_0 = \frac{1}{h_0}\left(\frac{L}{\pi}\right)^2 \tag{25}$$

The external bending moment M_e is expressed in Equation (26). Dependency of the stress at Point 2 and the strain at Point 2 on the strain at Point 1 is established in Equation (27):

$$M_e = N_e y_{tot} \tag{26}$$

$$\begin{gathered} M_i = M_e \rightarrow \sigma_2\beta - \sigma_1\beta = N_e y_{tot} \rightarrow \frac{\beta}{N_e}\left(\sigma_2 + \frac{N_e}{\alpha_1} + \frac{\alpha_2}{\alpha_1}\sigma_2\right) = y_{tot} \rightarrow \\ \frac{\beta}{N_e}\left[\sigma_2\left(1 + \frac{\alpha_2}{\alpha_1}\right) + \frac{N_e}{\alpha_1}\right] = y_0 + (\varepsilon_2 - \varepsilon_1)\chi_0 \rightarrow \\ \sigma_2\left(\beta + \beta\frac{\alpha_2}{\alpha_1}\right)\frac{1}{N_e} - \varepsilon_2\chi_0 = y_0 - \varepsilon_1\chi_0 - \frac{\beta}{\alpha_1} \end{gathered} \tag{27}$$

$$\begin{gathered} (a+b)^2 = a^2 + 2ab + b^2 \\ (a+b)\cdot(a-b) = a^2 - b^2 \end{gathered} \tag{1}$$

The relation between the stress at Point 2 σ_2 and the secant modulus $E_{s.fi}$ is approximated as in Equation (28):

$$\sigma_2 = \varepsilon_2 E_{s.fi} \tag{28}$$

$E_{s.fi}$ is formulated as Equations (29) and (30):

$$if\ \frac{N_e}{A_i} \leq f_{p.\theta} \rightarrow E_{s.fi} = E_{a.\theta} \tag{29}$$

$$if\ \frac{N_e}{A} > f_{p.\theta} \rightarrow \varepsilon_{fi} = \varepsilon_{y.\theta} - a_{EC}\sqrt{1 - \frac{1}{a_{EC}^2}\left(\frac{N_e}{A_i} + c_{EC} - f_{p.\theta}\right)^2} \rightarrow E_{s.fi} = \frac{N_e}{A\varepsilon_{fi}} \tag{30}$$

In case the stress from the axial load only is lower than the proportionality limit, the secant modulus is equal to the elasticity modulus for the temperature under consideration ($E_{a.\theta}$), as defined in Equation (29); in case the opposite is true, the secant modulus is calculated using Equation (30), where ε_{fi} is simply an inverse function to the EN 1993-1-2 [1] stress function in the inelastic range. Equation (23) can be rewritten into Equation (31):

$$\begin{gathered} -f_{p.\theta} + c_{EC} - \frac{b_{EC}}{a_{EC}}\sqrt{a_{EC}^2 - (\varepsilon_{y.\theta} + \varepsilon_1)^2} = -\frac{N_e}{\alpha_1} - \frac{\alpha_2}{\alpha_1}E_{s.fi}\varepsilon_2 \rightarrow \\ \sqrt{a_{EC}^2 - (\varepsilon_{y.\theta} + \varepsilon_1)^2} = \frac{a_{EC}}{b_{EC}}\frac{\alpha_2}{\alpha_1}E_{s.fi}\varepsilon_2 + \frac{a_{EC}}{b_{EC}}\left(\frac{N_e}{\alpha_1} - f_{p.\theta} + c_{EC}\right) \end{gathered} \tag{31}$$

Equation (28) is inserted into Equation (27), producing Equation (32), which is the dependence of the strain at Point 2 on the strain at Point 1:

$$\begin{gathered} E_{s.fi}\varepsilon_2\left(\beta + \beta\frac{\alpha_2}{\alpha_1}\right)\frac{1}{N_e} - \varepsilon_2\chi_0 = y_0 - \varepsilon_1\chi_0 - \frac{\beta}{\alpha_1} \rightarrow \\ \varepsilon_2\left[\left(\beta + \beta\frac{\alpha_2}{\alpha_1}\right)\frac{1}{N_e}E_{s.fi} - \chi_0\right] = y_0 - \varepsilon_1\chi_0 - \frac{\beta}{\alpha_1} \rightarrow \\ \varepsilon_2 = \frac{y_0 - \frac{\beta}{\alpha_1}}{\left(\beta + \beta\frac{\alpha_2}{\alpha_1}\right)\frac{1}{N_e}E_{s.fi} - \chi_0} - \varepsilon_1\frac{\chi_0}{\left(\beta + \beta\frac{\alpha_2}{\alpha_1}\right)\frac{1}{N_e}E_{s.fi} - \chi_0} \end{gathered} \tag{32}$$

Factors γ_0–γ_8 are used for convenience according to Equations (33)–(42):

$$\gamma_0 = \left(1 + \frac{\alpha_2}{\alpha_1}\right)\frac{\beta}{N_e}E_{s.fi} - \chi_0 \tag{33}$$

$$\gamma_1 = \frac{y_0 - \frac{\beta}{\alpha_1}}{\gamma_0} \tag{34}$$

$$\gamma_2 = \frac{\chi_0}{\gamma_0} \tag{35}$$

$$\gamma_3 = \frac{a_{EC}}{b_{EC}}\left(\frac{N_e}{\alpha_1} - f_{p.\theta} + c_{EC}\right) \tag{36}$$

$$\gamma_6 = 1 + \gamma_5^2 \tag{37}$$

$$\gamma_4 = \frac{a_{EC}}{b_{EC}}\frac{\alpha_2}{\alpha_1}E_{s.fi}\gamma_1 + \gamma_3 \tag{38}$$

$$\gamma_5 = \frac{a_{EC}}{b_{EC}}\frac{\alpha_2}{\alpha_1}E_{s.fi}\gamma_2 \tag{39}$$

$$\gamma_6 = 1 + \gamma_5^2 \tag{40}$$

$$\gamma_7 = 2\gamma_4\gamma_5 - 2\varepsilon_{y.\theta} \tag{41}$$

$$\gamma_8 = \gamma_4^2 - a^2 + \varepsilon_{y.\theta}^2 \tag{42}$$

Equation (32) is re-introduced as Equation (43):

$$\varepsilon_2 = \gamma_1 - \gamma_2\varepsilon_1 \tag{43}$$

Equation (43) is inserted into Equation (31), which, after transformation, results in a quadratic equation in relation to ε_1 in Equation (44):

$$\begin{gathered}
\sqrt{a_{EC}^2 - \left(\varepsilon_{y.\theta} + \varepsilon_1\right)^2} = \frac{a_{EC}}{b_{EC}}\frac{\alpha_2}{\alpha_1}E_{s.fi}(\gamma_1 - \gamma_2\varepsilon_1) + \gamma_3 \rightarrow \\
\sqrt{a_{EC}^2 - \left(\varepsilon_{y.\theta} + \varepsilon_1\right)^2} = \frac{a_{EC}}{b_{EC}}\frac{\alpha_2}{\alpha_1}E_{s.fi}\gamma_1 + \gamma_3 - \frac{a_{EC}}{b_{EC}}\frac{\alpha_2}{\alpha_1}E_{s.fi}\gamma_2\varepsilon_1 \rightarrow \\
\sqrt{a_{EC}^2 - \left(\varepsilon_{y.\theta} + \varepsilon_1\right)^2} = \gamma_4 - \gamma_5\varepsilon_1 \rightarrow \\
a_{EC}^2 - \varepsilon_{y.\theta}^2 + 2\varepsilon_{y.\theta}\varepsilon_1 - \varepsilon_1^2 = \gamma_4^2 - 2\gamma_4\gamma_5\varepsilon_1 + \gamma_5^2\varepsilon_1^2 \rightarrow \\
\varepsilon_1^2\left(1 + \gamma_5^2\right) - \varepsilon_1\left(2\gamma_4\gamma_5 - 2\varepsilon_{y.\theta}\right) + \left(\gamma_4^2 - a^2 + \varepsilon_{y.\theta}^2\right) = 0 \rightarrow \\
\gamma_6\varepsilon_1^2 - \gamma_7\varepsilon_1 + \gamma_8 = 0
\end{gathered} \tag{44}$$

The discriminant of Equation (44) is equal to Equation (45), and the roots can be found using (46). Equation (44) can have non-complex roots only if the discriminant (45) is non-negative:

$$D = \gamma_7^2 - \gamma_6\gamma_8 \tag{45}$$

$$\varepsilon_{1:1,2} = \frac{\gamma_7 \pm \sqrt{\gamma_7^2 - \gamma_6\gamma_8}}{2\gamma_6} \tag{46}$$

Equation (45) can be used to check the buckling condition: if Equation (45) is positive, stability is guaranteed; buckling load limit is obtained when Equation (45) is equal to 0.

Equation (45) can be rewritten using Equations (40)–(42), obtaining Equation (47), which is a simple quadratic equation in relation to γ_4:

$$\begin{gathered}\gamma_7^2 - 4\gamma_6\gamma_8 = 4\gamma_4^2\gamma_5^2 - 8\gamma_4\gamma_5\varepsilon_{y.\theta} + 4\varepsilon_{y.\theta}^2 - 4\left(1+\gamma_5^2\right)\left(\gamma_4^2 - a_{EC}^2 + \varepsilon_{y.\theta}^2\right) \rightarrow \\ \gamma_4^2 + 2\gamma_5\varepsilon_{y.\theta}\gamma_4 + \left[\gamma_5^2\left(\varepsilon_{y.\theta}^2 - a_{EC}^2\right) - a_{EC}^2\right] = 0\end{gathered} \tag{47}$$

The discriminant of Equation (47) is given by Equation (48), and the root with physical meaning is defined in Equation (49):

$$D = 4\gamma_5^2 a_{EC}^2 + 4a_{EC}^2 \tag{48}$$

$$\gamma_{4:1,2} = -\gamma_5\varepsilon_{y.\theta} + a_{EC}\sqrt{\gamma_5^2+1} \tag{49}$$

By equating Equations (38) and (49) and performing some transformations, it is possible to obtain Equation (50):

$$\begin{gathered}\frac{a_{EC}}{b_{EC}}\frac{\alpha_2}{\alpha_1}E_{s.fi}\gamma_1 + \gamma_3 = -\gamma_5\varepsilon_{y.\theta} + a_{EC}\sqrt{\gamma_5^2+1} \rightarrow \\ \frac{a_{EC}}{b_{EC}}\left(\frac{N_e}{\alpha_1} - f_{p.\theta} + c_{EC}\right) = -\gamma_5\varepsilon_{y.\theta} + a_{EC}\sqrt{\gamma_5^2+1} - \frac{a_{EC}}{b_{EC}}\frac{\alpha_2}{\alpha_1}E_{s.fi}\gamma_1 \rightarrow \\ N_e = \alpha_1\left[\frac{b_{EC}}{a_{EC}}\left(a_{EC}\sqrt{\gamma_5^2+1} - \frac{a_{EC}}{b_{EC}}\frac{\alpha_2}{\alpha_1}E_{s.fi}\gamma_1 - \gamma_5\varepsilon_{y.\theta}\right) + f_{p.\theta} - c_{EC}\right] \rightarrow \\ N_e = \alpha_1\left[b_{EC}\sqrt{\left(\frac{a_{EC}}{b_{EC}}\frac{\alpha_2}{\alpha_1}E_{s.fi}\frac{\chi_0}{\gamma_0}\right)^2 + 1} - \frac{\alpha_2}{\alpha_1}E_{s.fi}\varepsilon_{y.\theta}\frac{\chi_0}{\gamma_0} - \frac{\alpha_2}{\alpha_1}E_{s.fi}\frac{y_0 - \frac{\beta}{\alpha_1}}{\gamma_0} + f_{p.\theta} - c_{EC}\right]\end{gathered} \tag{50}$$

A direct solution of Equation (50) with reasonable effort is not possible, as $E_{s.fi}$ and γ_0 are both functions of N_e. Critical force is introduced as Equation (51) and the stability criteria is presented as Equation (52):

$$N_{cr.fi} = \alpha_1\left[b_{EC}\sqrt{\left(\frac{a_{EC}}{b_{EC}}\frac{\alpha_2}{\alpha_1}E_{s.fi}\frac{\chi_0}{\gamma_0}\right)^2 + 1} - \frac{\alpha_2}{\alpha_1}E_{s.fi}\varepsilon_{y.\theta}\frac{\chi_0}{\gamma_0} - \frac{\alpha_2}{\alpha_1}E_{s.fi}\frac{y_0 - \frac{\beta}{\alpha_1}}{\gamma_0} + f_{p.\theta} - c_{EC}\right] \tag{51}$$

$$N_e \leq N_{cr.fi} \tag{52}$$

The proposed method is based on a section shape consisting of rectangles (Figure 6). The actual section may deviate from the idealised area (e.g., chamfered corners of the SHS profiles). The idealised section area is denoted by A_i, while the actual section area is denoted by A. In case the design load is denoted by N_{fi}, N_e is defined as Equation (53):

$$N_e = N_{fi}\frac{A_i}{A} \tag{53}$$

Performance of the proposed method against non-linear FEM is demonstrated in Figure 7. The maximum limit buckling load $N_{cr.fi.max}$ was obtained numerically using Equation (51), satisfying condition in Equation (52). The buckling factor χ_{fi} was derived using Equation (54):

$$\chi_{fi} = \frac{N_{cr.fi.max}}{Af_{y.\theta}} \tag{54}$$

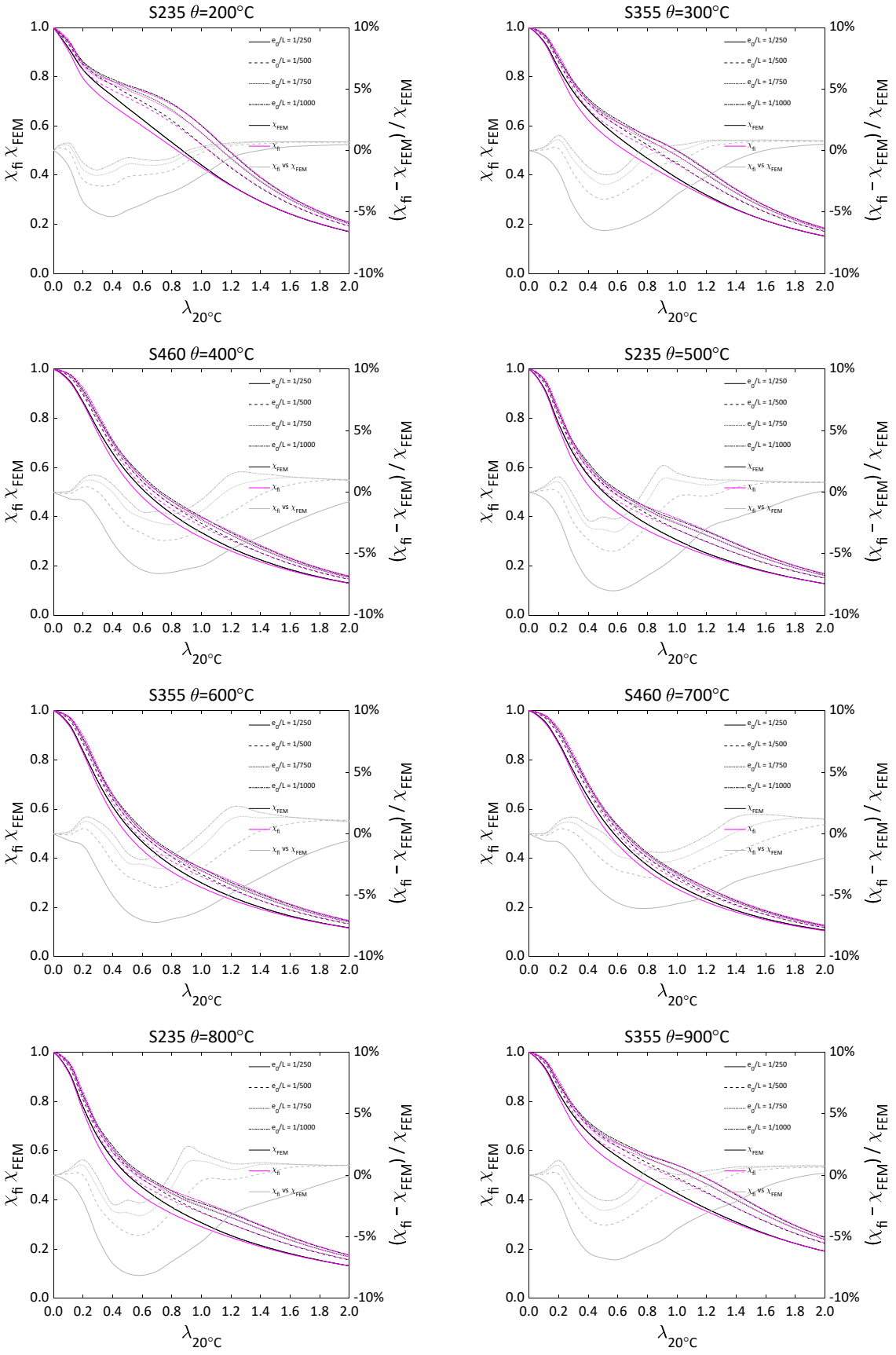

Figure 7. Performances of the proposed method against non-linear FEM for different steel grades, heating temperatures and initial imperfection values.

In Figure 7, the buckling factor χ_{fi} is compared to the buckling factor obtained by FEM χ_{FEM}. Performance was satisfactory for small-to-moderate initial imperfection values: $y_0 = L/1000 - L/500$. The performance of the method for a relatively large initial imperfection of $y_0 = L/250$ was judged to be unsatisfactory. According to the accepted approach, the initial imperfection of $y_0 = L/1000$ is used for buckling problems in fire conditions [24]. As the proposed model is intended to be used in reliability analysis where initial imperfection is one of the important parameters, the method was improved by introducing a fitting procedure. It was assumed that the main reason why the proposed method diverged from the non-linear FEM is the assumption of linear stress variation, as shown in Equation (8). The assumption was modified as follows: the factors α_1 and α_2 (Equations (14) and (15)) were redefined as Equations (55) and (56), where parameter g was introduced as a function of initial imperfection and slenderness:

$$\alpha_1 = gA \tag{55}$$

$$\alpha_2 = (1 - g)A \tag{56}$$

Parameter u was defined as Equation (57):

$$u = log\frac{L}{y_0} \tag{57}$$

The buckling capacity model with redefined α_1 and α_2 was fitted to a non-linear simulation data array. The non-linear FEM data array was formed from the results for temperature range θ = 200–900 °C, the slenderness range $\lambda_{20°C}$ = 0.1–2.0, the yield limit range 235–460 MPa and the initial imperfection range L/y_0 = 250–1000. The results of the fitting procedure were compiled into Equations (58)–(62):

$$g = \frac{p_1\lambda_{20°C}^2 + p_2\lambda_{20°C} + p_3}{\lambda_{20°C}^2 + q_1\lambda_{20°C} + q_2} \tag{58}$$

$$p_2 = -0.0525u^3 + 1.1054u^2 - 7.7123u + 17.4422 \tag{59}$$

$$p_3 = 0.0408u^3 - 0.7913u^2 + 5.0019u - 10.1146 \tag{60}$$

$$q_1 = -0.1143u^3 + 2.3736u^2 - 16.3483u + 36.4075 \tag{61}$$

$$q_2 = 0.0796u^3 - 1.5589u^2 + 9.9914u - 20.5392 \tag{62}$$

The performance of the updated model is demonstrated in Figure 8. The performance of the updated model against FEM was good. Therefore, the proposed method can be evaluated against EN 1993-1-2 [1] on the basis of Figure 2, where FEM and EN 1993-1-2 are compared. It is concluded that the proposed method provides improved accuracy compared to EN 1993-1-2.

As the proposed method has no direct analytical solution, the buckling capacity can be checked using one calculation cycle, but an iterative procedure is needed to define the buckling capacity limit. A simple line search algorithm can be used for this purpose. The buckling capacity model as shown in Equation (51) can be effectively used for reliability calculations using a Monte Carlo simulation, as the precise value of the capacity is not necessary and binary (0/1) type output is sufficient [26].

The calculation of the maximum buckling capacity limit by the proposed method was computationally efficient, demanding, on average, 2×10^{-5} s compared to the 2 s time for non-linear FEM procedure (8 cores 3.6 GHz). The computation time for the capacity verification was even shorter, approaching 10^{-6} s.

The procedure of the proposed method is summarised as follows:

1. Calculate the parameter u using Equation (57);
2. Calculate the parameters p_1, p_2, p_3, q_1 and q_2 using Equations (59)–(62);

3. Calculate the parameter g using Equation (58);
4. Calculate the parameters α_1 and α_2 using Equations (55) and (56);
5. Calculate the parameter β using Equation (20);
6. Calculate the secant modulus $E_{s,fi}$ using Equations (29) or (30) as:

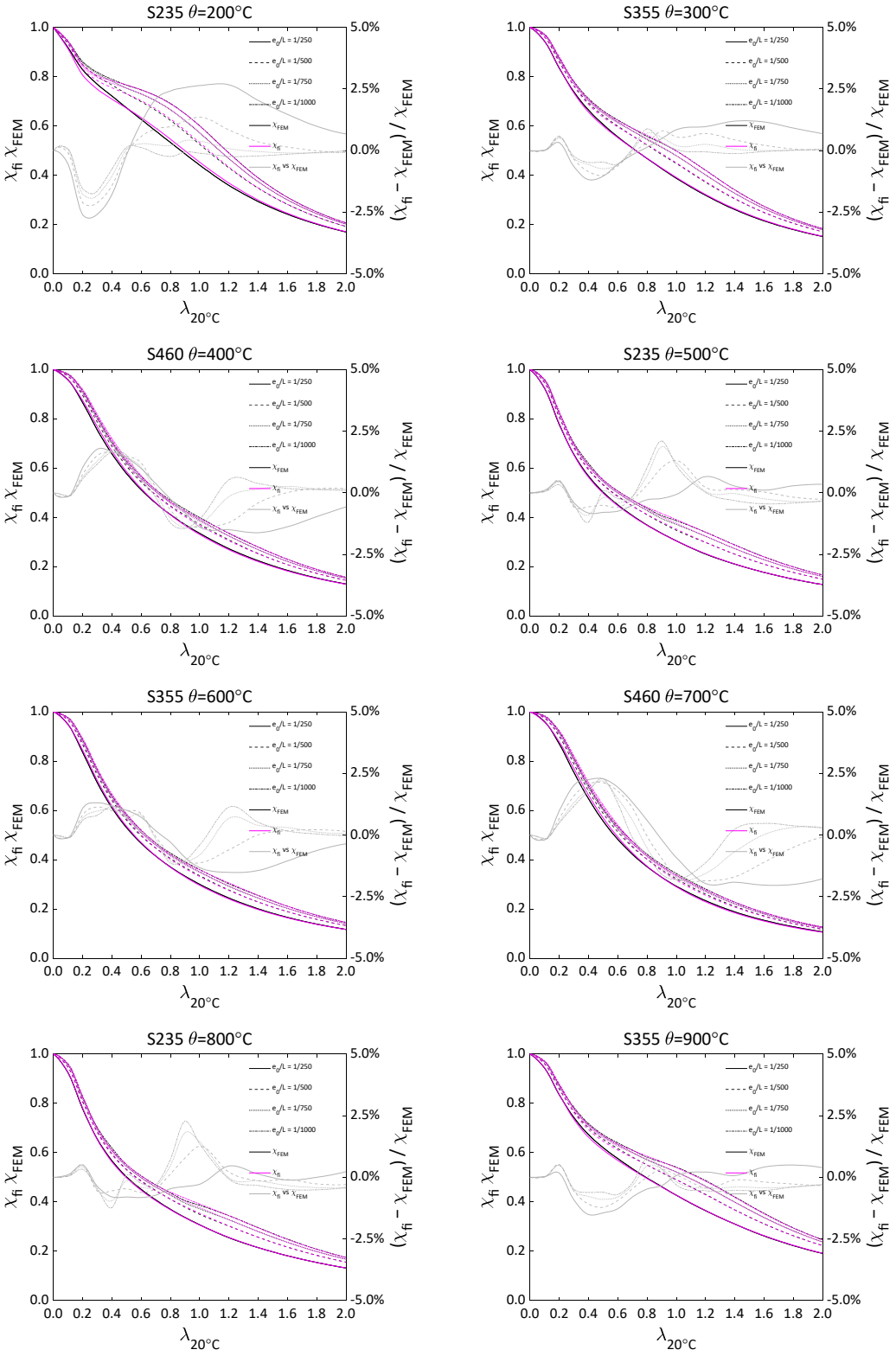

Figure 8. Performances of the proposed method against non-linear FEM after modification for different steel grades, heating temperatures and initial imperfection values.

$$if\ \frac{N_e}{A_i} \le f_{p.\theta} \rightarrow E_{s.fi} = E_{a.\theta}$$

$$if\ \frac{N_e}{A} > f_{p.\theta} \rightarrow \varepsilon_{fi} = \varepsilon_{y.\theta} - a_{EC}\sqrt{1 - \frac{1}{a_{EC}^2}\left(\frac{N_e}{A_i} + c_{EC} - f_{p.\theta}\right)^2} \rightarrow E_{s.fi} = \frac{N_e}{A\varepsilon_{fi}}$$

7. Calculate the model parameters χ_0 and γ_0 using Equations (25) and (33);
8. Calculate the EN 1993-1-2 [1] material model parameters a_{EC}, b_{EC} and c_{EC};
9. Calculate the critical force using Equation (52) as:

$$N_{cr.fi} = \alpha_1\left[b_{EC}\sqrt{\left(\frac{a_{EC}}{b_{EC}}\frac{\alpha_2}{\alpha_1}E_{s.fi}\frac{\chi_0}{\gamma_0}\right)^2 + 1} - \frac{\alpha_2}{\alpha_1}E_{s.fi}\varepsilon_{y.\theta}\frac{\chi_0}{\gamma_0} - \frac{\alpha_2}{\alpha_1}E_{s.fi}\frac{y_0 - \frac{\beta_1}{\alpha_1}}{\gamma_0} + f_{p.\theta} - c_{EC}\right]$$

10. Check the buckling capacity:

$$\text{If } N_e \le N_{cr.fi} \rightarrow \text{stability guaranteed.}$$

5. Example

In order to demonstrate the proposed method, a calculation example is presented.
Section: SHS200 × 6.0
Steel grade: S355 -> f_y = 355 MPa, E = 210,000 MPa
Temperature: θ = 500 °C
Effective length: L_{eff} = 3010 mm -> $\lambda_{20°C}$ = 0.5
Section parameters: A = 4560 mm^2, I_y = 2.83 × 10^7 mm^4
Axial load: N_{fi} = 720 kN
Initial imperfection: y_0 = 6.0 mm
$k_{y,\theta}$ = 0.780, $k_{p,\theta}$ = 0.360, $k_{E,\theta}$ = 0.600, $\varepsilon_{p,\theta}$ = 0.0010143, $\varepsilon_{y,\theta}$ = 0.02, $f_{y,\theta}$ = 276.9 MPa
$f_{p,\theta}$ = 127.8 MPa, $E_{a,\theta}$ = 126,000 MPa

$$\overline{\lambda} = \frac{L_{eff}}{\sqrt{\frac{I_y}{A}}\pi}\sqrt{\frac{f_y}{E}} = \frac{3010}{\sqrt{\frac{2.83\times10^7}{4560}}\pi}\sqrt{\frac{355}{210000}} = 0.4948$$

$$\overline{\lambda_\theta} = \overline{\lambda}\sqrt{\frac{k_{y,\theta}}{k_{E,\theta}}} = 0.4948\sqrt{\frac{0.780}{0.600}} = 0.5642$$

Eurocode method:
Notation from EN 1993-1-2 [1] is used.

$$\alpha = 0.65\sqrt{\frac{235}{f_y}} = 0.65\sqrt{\frac{235}{355}} = 0.529$$

$$\varphi_\theta = \frac{1}{2}\left[1 + \alpha\overline{\lambda_\theta} + \overline{\lambda_\theta}^2\right] = \frac{1}{2}\left[1 + 0.529 \times 0.5642 + 0.5642^2\right] = 0.8084$$

$$\chi_{fi} = \frac{1}{\varphi_\theta + \sqrt{\varphi_\theta{}^2 - \overline{\lambda_\theta}^2}} = \frac{1}{0.8084 + \sqrt{0.8084^2 - 0.5642^2}} = 0.7208$$

$$N_{b,fi,t,Rd} = \chi_{fi}Ak_{y,\theta}f_y = 0.7208 \times 4560 \times 0.780 \times 355 = 910,130\ N$$

FEM:
Buckling resistance obtained by the FEM procedure described in Section 3.

$$N_{fi.FEM} = 736,260\ N$$

Proposed method:
Section geometrical parameters from Figure 6:

$$h_0 = 200 - 6 = 194 \text{ mm} h = 200 - 2 \times 6 = 188 \text{ mm}$$

Calculate the parameter u using Equation (57):

$$u = log\frac{L}{y_0} = log\frac{3010}{6} = 6.2178$$

Calculate the parameters p_1, p_2, p_3, q_1 and q_2 using Equations (59)–(62):

$$p_1 = -0.0128u^3 + 0.2431u^2 - 1.5429u + 3.725 = 0.4531$$

$$p_2 = 0.0525u^3 + 1.1054u^2 - 7.7123u + 17.4422 = -0.3957$$

$$p_3 = 0.0408u^3 - 0.7913u^2 + 5.0019u - 10.1146 = 0.2015$$

$$q_1 = 0.1143u^3 + 2.3736u^2 - 16.3483u + 36.4075 = -0.9533$$

$$q_2 = 0.0796u^3 - 1.5589u^2 + 9.9914u - 20.5392 = 0.4514$$

Calculate the parameter g using Equation (59):

$$g = \frac{p_1\lambda_{20°C}^2 + p_2\lambda_{20°C} + p_3}{\lambda_{20°C}^2 + q_1\lambda_{20°C} + q_2} = 0.5202$$

Calculate the parameters α_1 and α_2 using Equations (55) and (56):

$$\alpha_1 = gA = 2372 \text{ mm}^2$$

$$\alpha_2 = (1-g)A = 2188 \text{ mm}^2$$

Calculate the parameter β using Equation (20):

$$\beta = bt\frac{h_0}{2} + \frac{h^2 t}{12} = 151,744 \text{ mm}^3$$

Calculate the EN 1993-1-2 [1] material model parameters a_{EC}, b_{EC} and c_{EC}:

$$a_{EC} = 0.019 \;\; b_{EC} = 159.716 \;\; c_{EC} = 10.616$$

Calculate the secant modulus $E_{s.fi}$ using Equations (29) or (30):

$$\frac{N_e}{A} = 157.9\ MPa > f_{p.\theta} = 127.8\ MPa \rightarrow \varepsilon_{fi} = \varepsilon_{y.\theta} - a_{EC}\sqrt{1 - \frac{1}{a_{EC}^2}\left(\frac{N_e}{A_i} + c_{EC} - f_{p.\theta}\right)^2} = 0.0016 \rightarrow$$

$$E_{s.fi} = \frac{N_e}{A\varepsilon_{fi}} = 98,640\ MPa$$

Calculate the model parameters χ_0 and γ_0 using Equations (25) and (33):

$$\chi_0 = \frac{1}{h_0}\left(\frac{L}{\pi}\right)^2 = 4731 \quad \gamma_0 = \left(1 + \frac{\alpha_2}{\alpha_1}\right)\frac{\beta}{N_e}E_{s.fi} - \chi_0 = 35,231$$

Calculate the critical force using Equation (51):

$$N_{cr.fi} = \alpha_1\left[b_{EC}\sqrt{\left(\frac{a_{EC}}{b_{EC}}\frac{\alpha_2}{\alpha_1}E_{s.fi}\frac{\chi_0}{\gamma_0}\right)^2 + 1} - \frac{\alpha_2}{\alpha_1}E_{s.fi}\varepsilon_{y.\theta}\frac{\chi_0}{\gamma_0} - \frac{\alpha_2}{\alpha_1}E_{s.fi}\frac{y_0 - \frac{\beta_1}{\alpha_1}}{\gamma_0} + f_{p.\theta} - c_{EC}\right] = 722,510\ N$$

Check the buckling capacity:

$$N_e = 720,000\ N < N_{cr.fi} = 722,510\ N \rightarrow \text{stability guaranteed.}$$

The presented method enables us to check the buckling capacity with the given axial force. As the critical force $N_{cr.fi}$ itself is dependent on the axial force N_e, the maximum buckling capacity $N_{cr.fi.max}$ can be calculated iteratively or by increasing stepwise the axial load N_e until $N_e = N_{cr.fi}$. In this example, the maximum buckling capacity calculated using the proposed method is $N_{cr.fi.max}$ = 724,610 N, which is very close to the buckling capacity calculated using nonlinear FEM, $N_{fi.FEM}$ = 736,260 N (the difference is 1.6%).

6. Conclusions

A new engineering method for evaluating the buckling resistance of RHS and SHS columns with compact cross sections in fire has been proposed. The procedure enables us to assess the resistance of columns in a wide range of temperatures and structural parameters, such as slenderness, steel grades and initial imperfection. In developing the method, distribution of stresses at buckling was analysed in detail. As shown, the bending stiffness of the column is a key parameter affecting the buckling process, and in elevated temperature conditions, the reduction path of the stiffness in the buckling process is more complex than in normal temperature conditions. Buckling factors obtained in the proposed scheme were compared with the values calculated by the current EN 1993-1-2 [1] method.

The presented method provides improved accuracy compared to Eurocode, which appears to be unconservative in certain ranges of parameters. The method is validated by extensive numerical simulation program. Besides the improved accuracy, the main advantage of the proposed approach is computational efficiency, which is essential for the emerging probabilistic and data-set based design methods demanding high numbers of repeated calculations. The computational time of the new technique overweighs by order of magnitude the relevant expenditure by FEM. The potential of the method for probability-based analysis is supported by the format, which enables us to explicitly handle the uncertainties of essential parameters.

The presented framework is suitable for incorporating different material models and extending the range of section geometries consisting of flat elements, e.g. I or H sections. Stainless steel and high strength steel columns can be handled in the future development of the method.

Author Contributions: Conceptualization, A.K. and I.T.; methodology, A.K. and I.T.; software, A.K.; formal analysis, A.K.; writing—original draft preparation, A.K. and I.T.; writing—review and editing, A.K. and I.T. All authors have read and agreed to the published version of the manuscript.

Funding: This research received no external funding.

Data Availability Statement: Data sharing is not applicable to this article.

Conflicts of Interest: The authors declare no conflict of interest.

References

1. European Committee for Standardization. *Eurocode 3 Design of Steel Structures—Part 1–2: General Rules—Structural Fire Design*; European Committee for Standardization: Brussels, Belgium, 2005.
2. Franssen, J.M.; Talamona, D.; Kruppa, J.; Cajot, L.G. Stability of steel columns in case of fire: Experimental evaluation. *J. Struct. Eng.* **1998**, *124*, 156–163. [CrossRef]
3. Talamona, D.; Franssen, J.M.; Schleich, J.; Kruppa, J. Stability of steel columns in case of fire: Numerical modelling. *J. Struct. Eng.* **1997**, *123*, 713–720. [CrossRef]
4. Knobloch, M.; Somaini, D.; Pauli, J.; Fontana, M. Stability of steel columns in fire. In Proceedings of the International Colloquium Stability and Ductility of Steel Structures, Rio de Janeiro, Brazil, 8–10 September 2010; pp. 465–472.
5. Somaini, D.; Knobloch, M.; Fontana, M. Buckling of steel columns in fire: Non-linear behaviour and design proposal. *Steel Constr. Des. Res.* **2012**, *5*, 175–182. [CrossRef]

6. Vila Real, P.M.M.; Lopes, N.; da Silva, L.S.; Piloto, P.A.G.; Franssen, J.M. Numerical modelling of steel beam-columns in case of fire—Comparison with Eurocode 3. *Fire Saf. J.* **2004**, *39*, 23–39. [CrossRef]
7. Toh, W.; Tan, K.; Fung, T. Compressive resistance of steel columns in fire: Rankine approach. *J. Struct. Eng.* **2000**, *126*, 398–405. [CrossRef]
8. Kervalishvili, A.; Talvik, I. Alternative approach to buckling of square hollow section steel columns in fire. *J. Constr. Steel Res.* **2014**, *96*, 140–150. [CrossRef]
9. Ricardo, A.S.; Gomes, W.J.S. Structural reliability methods applied in analysis of steel elements subjected to fire. *J. Eng. Mech.* **2021**, *147*, 04021108. [CrossRef]
10. Qureshi, R.; Hopkin, C.D.; Gernay, T.; Khorasani, N.E. Reliability assessment of the US prescriptive standard for steel columns under fire. *Structures* **2022**, *40*, 711–724. [CrossRef]
11. Jindra, D.; Kala, Z.; Kala, J. Flexural buckling of stainless steel CHS columns: Reliability analysis utilizing FEM simulations. *J. Constr. Steel Res.* **2022**, *188*, 107002. [CrossRef]
12. Guo, Q.; Jeffers, A.E. Finite-element reliability analysis of structures subjected to fire. *J. Struct. Eng.* **2014**, *141*, 04014129. [CrossRef]
13. Vasileiou, A.S.; Anyfantis, K.N. Reliability analysis of SHS compression members in shipbuilding: Derivation of probabilistic buckling curves. *Ships Offshore Struct.* **2022**. *ahead-of-print*. [CrossRef]
14. Rad, M.M.; Habashneh, M.; Lógó, J. Elasto-Plastic limit analysis of reliability based geometrically nonlinear bi-directional evolutionary topology optimization. *Structures* **2021**, *34*, 1720–1733. [CrossRef]
15. Tong, Q.; Couto, C.; Gernay, T. Machine learning models for predicting the resistance of axially loaded slender steel columns at elevated temperatures. *Eng. Struct.* **2022**, *166*, 114620. [CrossRef]
16. Balogh, T.; Vigh, L.G. Complex and comprehensive method for reliability calculation of structures under fire exposure. *Fire Saf. J.* **2016**, *86*, 41–52. [CrossRef]
17. Szalai, J.; Papp, F. On the theoretical background of the generalization of Ayrton-Perry type resistance formulas. *J. Constr. Steel Res.* **2010**, *66*, 670–679. [CrossRef]
18. Ayrton, W.; Perry, J. On Struts. *Engineer* **1886**, *62*, 464–465.
19. Schleich, J.; Gayot, L.G.; Kruppa, J.; Talamona, D.; Azpizau, W.; Unanue, J.; Twilt, L.; Fellinger, J.; Van Foeken, R.; Franssen, J.M. Buckling curves of hot rolled H steel sections submitted to fire. In *Technical Steel Research*; C.E.C.: Brussels, Belgium, 1998.
20. Maślak, M. Rankine-Merchant Approach to specification of flexural buckling coefficient for fire situation. *J. Civ. Eng. Archit.* **2012**, *6*, 1302–1309. [CrossRef]
21. Neves, I.C.; Valente, J.C.; Rodrigues, J.P.C. Thermal restraint and fire resistance of columns. *Fire Saf. J.* **2002**, *37*, 753–771. [CrossRef]
22. Wang, P.; Li, G.; Wang, Y. Behaviour and design of restrained steel column in fire, Part 3: Practical design method. *J. Constr. Steel Res.* **2010**, *66*, 1422–1430. [CrossRef]
23. Karman, T. Unteruschungen über Knickfestigkeit. *Ver. Dtsch. Ing.* **1910**, *81*, 1–44.
24. ECCS Techinal Comitee 8. *Structural Stability—Manual on Stability*, 2nd ed.; ECCS: DeLand, FL, USA, 1976.
25. Pauli, J. *The Behaviour of Steel Columns in Fire: Material—Cross-Sectional Capacity—Column Buckling*; Institut für Baustatik und Konstruktion der ETH: Zürich, Switzerland, 2012.
26. Kervalishvili, A.; Talvik, I. Reliability based design method for buckling of steel columns in fire. *J. Struct. Fire Eng.* **2019**, *11*, 167–187. [CrossRef]